

Linking high-energy cosmic particles by black hole jets embedded in large-scale structures

Ke Fang¹ and Kohta Murase²

¹*Department of Astronomy; Joint Space-Science Institute,
University of Maryland, College Park, MD, 20742-2421, USA*

²*Department of Physics; Department of Astronomy and
Astrophysics; Center for Particle and Gravitational Astrophysics,
The Pennsylvania State University, University Park, Pennsylvania 16802, USA*

The origin of ultrahigh-energy cosmic rays (UHECRs) has been a half-century old enigma [1]. The mystery has been deepened by an intriguing coincidence that with ten orders of magnitude across the energy, the energy generation rates of UHECRs, PeV neutrinos, and isotropic sub-TeV γ rays are comparable, hinting at a grand-unified picture [2]. Here we report that powerful black hole jets inhabited in aggregates of galaxies can work as their common origins. Once accelerated by a jet, low-energy cosmic rays confined in the radio lobe are adiabatically cooled; higher-energy cosmic rays leaving the source interact with the magnetized cluster environment and produce neutrinos and γ rays; the highest-energy particles escape from the host cluster and contribute to the observed cosmic rays above 0.1 EeV. The model is consistent with the spectrum, composition, and isotropy of the observed UHECRs, while explaining the IceCube neutrinos and the non-blazar component of the Fermi γ -ray background, with a reasonable energy output from black hole jets in clusters.

The origin of ultrahigh-energy cosmic rays (UHECRs) is still unknown [1]. Measurements by the Pierre Auger Observatory (Auger) [3] and the Telescope Array (TA) [4] find a power-law spectrum, $dN/dE \sim E^{-2.6} - E^{-2.7}$, with a decline above 60 EeV, probably due to the interaction of UHECRs with the cosmic microwave background (CMB) or an upper limit of the particle energy reachable by the accelerator. Small-scale anisotropy in their arrival directions has not been established [3, 4].

The IceCube Observatory recently discovered high-energy cosmic neutrinos [5, 6], which have been anticipated to provide crucial clues to this age-old mystery. An astrophysical flux in the 0.1-1 PeV range is found at the level of $10^{-8} \text{ GeV}^{-1} \text{ cm}^{-2} \text{ s}^{-1} \text{ sr}^{-1}$ per flavor [5, 7], which is consistent with expectations of cosmic-ray “reservoir” models [8–11]. The arrival directions of the observed events present no significant clustering, and indicate that the sources are extragalactic [5, 7, 12].

A γ -ray counterpart is expected from the hadronic processes responsible for neutrino production. If the source environment is transparent to γ rays, these side products should show up at 1-100 GeV energies after cascading in the extragalactic background light (EBL). A significant fraction of the extragalactic γ -ray background (EGB) [13, 14] measured by the Fermi Gamma-Ray Space Telescope may be explained by neutrino sources [11]. Despite the unknown origins of these multi-messenger emissions and fine structures in their data (such as a possible excess in the 10-100 TeV neutrino spectrum [5]), it is remarkable that with over ten orders of magnitude in energy, energy generation rates of UHECRs, IceCube neutrinos, and Fermi EGB are all comparable [2, 11, 12].

Recent UHECR observations have revealed more characteristic features of extragalactic cosmic rays. First, a hardening in the spectrum of light particles is seen around 0.1 EeV [15, 16], right in the energy range where a steepening in the spectrum of heavy primary particles is observed (which is often referred as the “second knee”). Second, a transition from light elements to medium-to-heavy elements around 10 EeV has been suggested by the Auger data [3], and heavy UHECR composition is also supported by the non-detection of cosmogenic neutrinos [17]. Although the interpretation of the UHECR composition is still under debate, direct measurements of the indicator of the particle mass seem to be consistent between different experiments. These features were not considered by the simplest convergence theory [2], and we here provide a concrete astrophysical model by which black hole jets embedded in large-scale structures reconcile these observations.

Relativistic jets from the accretion onto supermassive black holes provide promising sites for UHECR acceleration. The Hillas condition suggests that jets of an active galactic nucleus (AGN) can accelerate a particle with charge Z to a maximum energy, $E_{\max} \sim Z 10^{19} \text{ eV}$ [18–20]. The energy spectrum of particles accelerated by the Fermi mechanism can be described by a power law, $dN_{\text{acc}}/dE \propto E^{-s_{\text{acc}}}$, with an index $s_{\text{acc}} \sim 2 - 2.5$. Radio observations often find extended lobes (sometimes referred as bubbles or cocoons, which are plasma cavities inflated by the jet), with 10 – 100 kiloparsec scales [21] and 0.1–10 microgauss-level magnetic fields [22]. Particles with energy below $E_{\text{lobe},c} = Z e B_{\text{lobe}} l_{\text{lobe},c} \sim 1.4 Z (B_{\text{lobe}}/5 \mu\text{G}) (l_{\text{lobe},c}/0.3 \text{ kpc}) \text{ EeV}$ have a Larmor radius $r_L = E/(ZeB)$ much smaller than the coherence length of their magnetic structure, where B_{lobe} and $l_{\text{lobe},c} \sim 0.01 - 0.1 r_{\text{lobe}}$ are the magnetic field strength and the coherence length, and r_{lobe} is the lobe size. These particles diffuse for $t_{\text{diff}}^{\text{lobe}} \sim 6.1 (r_{\text{lobe}}/10 \text{ kpc})^2 (E/Z 1 \text{ PeV})^{-1/3} (l_{\text{lobe},c}/0.3 \text{ kpc})^{-2/3} (B_{\text{lobe}}/5 \mu\text{G})^{1/3} \text{ Myr}$ before entering the intracluster medium (ICM). Meanwhile, they suffer from adiabatic losses due to the expansion of the cocoon. The characteristic cooling time is $t_{\text{ad}} \sim 4.9 (r_{\text{lobe}}/10 \text{ kpc}) (v_{\text{lobe}}/2000 \text{ km s}^{-1})^{-1} \text{ Myr}$, with v_{lobe} being the typical expansion velocity at a source age $\sim 0.1 - 10 \text{ Myr}$ [23]. Particles with energy above $E_{\text{lobe},c}$ are less impacted, escaping semi-diffusively with $t_{\text{diff}}^{\text{lobe}} \propto E^{-2}$. Considering the competition between diffusion and cooling, we approximate the spectrum of cosmic rays leaking into the cluster to be $dN_{\text{inj}}/dE \propto E^{-s_{\text{acc}}} \exp(-t_{\text{diff}}^{\text{lobe}}/t_{\text{ad}})$.

Radio-loud AGNs preferentially reside around the center of rich clusters [24]. A cluster with a halo mass of $M = 10^{14} M_{14} M_{\odot}$ has a virial radius $r_{\text{vir}} \sim 1.2 M_{14}^{1/3} \text{ Mpc}$. The distribution of thermal gas is often described by the β model as $n_{\text{ICM}}(r) \propto [1 + (r/r_c)^2]^{-3\beta/2}$, where $\beta \approx 0.8$ and $r_c \sim 0.1 r_{\text{vir}}$ is the core radius [25]. Turbulent magnetic fields in the ICM, probably induced by accretion shocks and other cluster dynamics, typically have a strength of a few μG in the cluster center [25]. Assuming that the field traces the baryon distribution through the flux conservation, we adopt a magnetic field profile, $B(r) = B_0 [1 + (r/r_c)^2]^{-\beta}$ with $B_0 \sim 5 \mu\text{G}$.

Cosmic rays leaving the lobe enter the ICM of the host cluster. The highest-energy particles travel rectilinearly through the ICM. Particles reaching an energy $E_c \sim 2 \times 10^{19} Z B_{-6} (l_c/20 \text{ kpc}) \text{ eV}$ have a gyro-radius comparable to the typical scales of magnetic field fluctuations in massive clusters, with l_c about 1-10% of the virial radius [25]. Particles with energies well below E_c diffusive propagate in the turbulent magnetic field of the cluster. The confinement, which could last for $\sim 1 - 10 \text{ Gyr}$, leads to efficient interactions of cosmic-ray nuclei with baryons of the ICM and infrared background photons in the cluster, producing pions that decay into neutrinos and γ rays via $\pi^{\pm} \rightarrow \nu_e(\bar{\nu}_e) + e^{\pm} + \nu_{\mu} + \bar{\nu}_{\mu}$ and $\pi^0 \rightarrow 2\gamma$, respectively. Finally, particles that successfully leave the cluster propagate to the Earth through the intergalactic medium. UHECRs from the sources beyond the energy-loss horizon are depleted via photodisintegration, photomeson production, and Bethe-Heitler pair production processes with the CMB and the EBL, producing cosmogenic neutrinos peaked around EeV and γ rays that cascade down to GeV-TeV energies.

We numerically simulate the propagation of UHECRs in the magnetized ICM and from the source to the observer. We assume that a jetted source locates randomly in the core of a cluster with uniformly probability. To give a generic example, we inject two types of elements: protons and iron nuclei, following the same power-law spectrum with a cutoff above the maximum rigidity, $dN_{\text{inj}}/dR \propto R^{-s_{\text{acc}}} \exp(-R/R_{\max})$, where $R = E/Ze$ is the rigidity, $s_{\text{acc}} = 2.3$, and $E_{\max} = Z 10^{19.4} \text{ eV}$. We let 83% of the total energy channelled into protons and the rest into iron nuclei. We assume that particles are confined up to $t_{\text{inj}} = 2 \text{ Gyr}$, considering that the peak period of AGN activities effectively lasts for $\sim 2 - 3 \text{ Gyr}$. (see Appendix for alternative scenarios and discussions on model uncertainties). The redshift evolution of the source density is taken to be $(1+z)^3$ up to $z_c = 1.5$, but its moderate variations barely impact our results. The cumulative flux is obtained

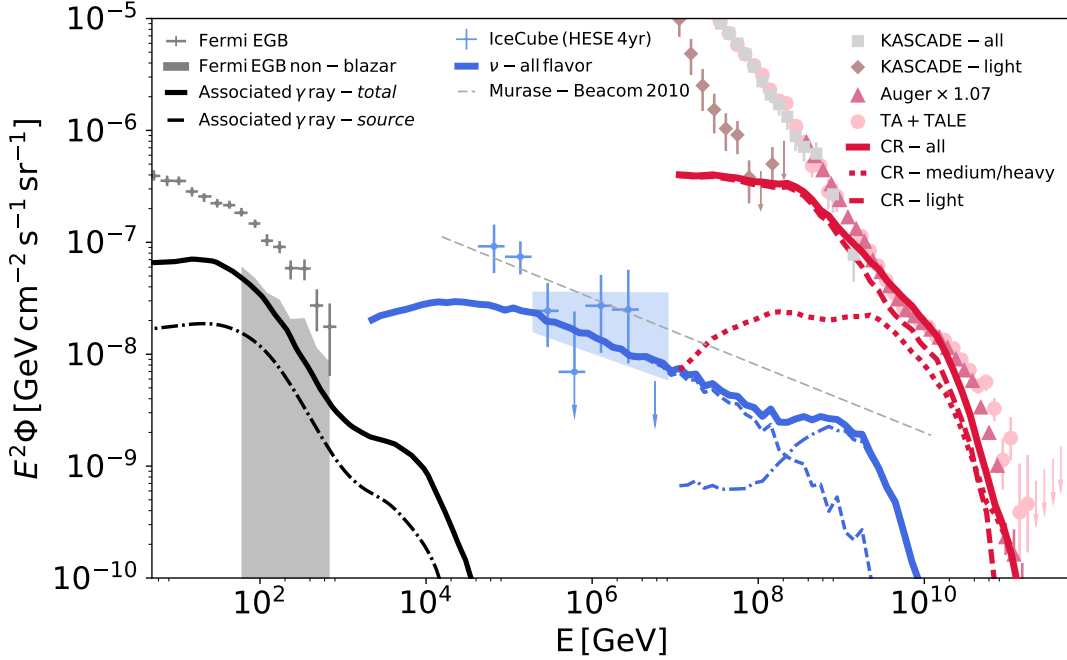


FIG. 1: Integrated spectra of cosmic rays, neutrinos, and γ rays from galaxy clusters and groups with black hole jets as accelerators, compared to measurements from the KASCADE-Grande [15], Telescope Array and Telescope Array Low Energy extension (TALE) [4], Pierre Auger observatory [3] (with energy scaled up by 7% to match TA data at the ankle), IceCube [7], and Fermi Gamma-Ray Space Telescope [13, 14]. The total cosmic ray spectrum (solid red) is decomposed into two composition groups: light (dashed red; H and He) and medium-heavy (dotted red; CNO, Si, Mg, Fe). PeV neutrinos (solid blue) are produced by interactions between cosmic rays and the ICM (dashed blue), and by UHECRs interacting with the CMB and EBL during their intergalactic propagation (dash-dotted blue). The upper bound on the neutrino flux of UHECR nuclei (for $s_{\text{acc}} = 2.3$) is shown for reference (dashed grey) [26]. The γ -ray counterparts (solid black for the total flux and dash-dotted black for γ rays produced in the ICM) are comparable to the non-blazar component of the EGB measured by the Fermi Gamma-Ray Space Telescope [14].

by [8]:

$$\Phi(E) = \frac{1}{4\pi} \int \frac{c dz}{H(z)} \int_{M_{\min}}^{\infty} dM \frac{dn}{dM} \frac{d\dot{N}}{dE'}(M, z), \quad (1)$$

where dn/dM is the halo mass function, $H(z)$ is the Hubble parameter at redshift z , $d\dot{N}/dE'$ is the production rate of neutrinos (or propagated cosmic rays) from a given cluster with a redshifted energy $E' = (1+z)E$. We consider clusters with a halo mass above $M_{\min} = 5 \times 10^{13} M_{\odot}$ (corresponding to $\sim 10^{11} M_{\odot}$ stellar mass), which present higher radio-loud AGN fractions [24].

Figure 1 shows the integrated spectra of UHECRs and neutrinos from over-density regions with black hole jets. The observed UHECR spectrum is normalized to the Auger data point at $10^{19.05}$ eV. The cosmic-ray confinement in the lobe and the host cluster makes the injection spectrum harder below the second knee [8, 11]. The spectral shape is in agreement with both measurements by Auger and TA above 10^{18} eV. Primary and secondary cosmic-ray particles received by the observer are divided into two composition groups: light (including H and He) and intermediate/heavy (including CNO, Si, Mg, Fe), with the two crossing around $10^{19.5}$ eV. The mean of the maximum depth of an air shower, $\langle X_{\max} \rangle$, which depends on the mass of the UHE nucleon or nucleus, is shown in

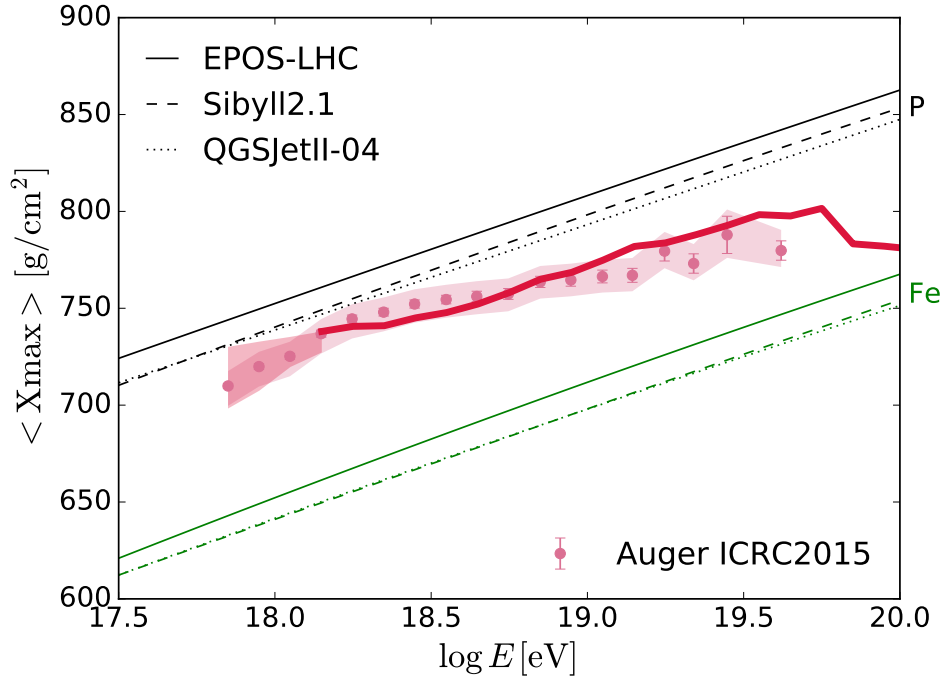


FIG. 2: The mean depth of the air-shower maximum, $\langle X_{\max} \rangle$, of the UHECRs in Fig 1 (solid red line, calculated with the EPOS interaction model [27]), comparing to that of the Auger data [3] (light red data points with the shaded region indicating systematic errors). For reference, $\langle X_{\max} \rangle$ of a 100% proton (black) and 100% iron nuclei composition (green) are shown, computed using three interaction models, EPOS, QGSJET, and SIBYLL, as listed in the legend box. The red shaded region indicates the energy range where the extragalactic contribution is less than 90% of the measured flux, and is determined by assuming that the residual flux, which could be a Galactic component, has a composition between proton and iron.

Figure 2. The trend follows the $\langle X_{\max} \rangle$ data measured by Auger. Below 10^{18} eV, the predicted cosmic-ray spectrum matches the light component of the KASCADE-Grande data [15].

The neutrino spectrum is composed of two parts. Between 10^{14} eV and 10^{17} eV, it is mostly contributed by particle interactions in the ICM. It meets the IceCube measurements above 10^{14} eV. The low-energy neutrino spectrum is harder than that of accelerated cosmic rays, and the spectral steepening above 10^{15} eV results from the faster escape of higher-energy cosmic rays. Above 10^{18} eV, the neutrino flux is dominated by the cosmogenic neutrinos produced when UHECRs interact with the CMB and the EBL, and is consistent with the IceCube constraints at extremely high energies [17]. Likewise, the observed sub-TeV γ rays are produced *both* in the ICM and during the intergalactic propagation [2]. Thanks to the hard injection spectrum, the total γ -ray flux largely originates from electromagnetic cascades, and is consistent with the non-blazar component of the EGB [14]. In addition to the hard γ -ray spectrum, our model also predicts a dominance of low-mass clusters, and the γ -ray and radio limits from individual clusters [28] can be satisfied.

The chance of previously or currently having active jets in a cluster, f_{jet} , and the average cosmic-ray luminosity of contained active galaxies per cluster, L_{CR} , are left as free parameters. Assuming $L_{\text{CR}} \sim 10^{44} - 10^{45} \text{ erg s}^{-1}$, we obtain $f_{\text{jet}} \sim 10\%$. This is consistent with duty cycles of the accretion-driven evolution of black holes [29]. The number density of clusters and groups with a mass above $5 \times 10^{13} M_{\odot}$ is $\sim 3 \times 10^{-5} \text{ Mpc}^{-3}$. This satisfies the muon neutrino limits on the neutrino source density derived from the absence of multiplets [2], as well as the lower bounds on the UHECR source density derived from the lack of strong anisotropy in the UHECR data [30].

Acknowledgments

We thank Rafael Alves Batista, Chris Reynolds and Michael Unger for helpful comments. This work made use of supercomputing resources at the University of Maryland. We gratefully acknowledge support from the Eberly College of Science of Penn State University and the Institute for Gravitation and the Cosmos. The work of K.M. is supported by NSF grant No. PHY-1620777.

-
- [1] K. Kotera and A. V. Olinto, *Ann.Rev.Astron.Astrophys.* **49**, 119 (2011), 1101.4256.
 - [2] K. Murase and E. Waxman, *PRD* **94**, 103006 (2016), 1607.01601.
 - [3] A. Aab et al. (Pierre Auger Collaboration) (2015), 1509.03732.
 - [4] J. Charles et al. (Telescope Array Collaboration), *Proceedings of Science (ICRC2015)* 035 (????).
 - [5] F. Halzen, *Nature Phys.* **13**, 232 (2016).
 - [6] M. Aartsen et al. (IceCube Collaboration), *Phys.Rev.Lett.* **111**, 021103 (2013), 1304.5356.
 - [7] M. G. Aartsen et al. (IceCube), *Astrophys. J.* **833**, 3 (2016), 1607.08006.
 - [8] K. Murase, S. Inoue, and S. Nagataki, *Astrophys.J.* **689**, L105 (2008), 0805.0104.
 - [9] K. Kotera, D. Allard, K. Murase, J. Aoi, Y. Dubois, et al., *Astrophys.J.* **707**, 370 (2009), 0907.2433.
 - [10] A. Loeb and E. Waxman, *JCAP* **0605**, 003 (2006), astro-ph/0601695.
 - [11] K. Murase, M. Ahlers, and B. C. Lacki, *Phys. Rev.* **D88**, 121301 (2013), 1306.3417.
 - [12] E. Waxman (2013), 1312.0558.
 - [13] M. Ackermann, M. Ajello, A. Albert, et al., *ApJ* **799**, 86 (2015), 1410.3696.
 - [14] M. Ackermann, M. Ajello, A. Albert, W. B. Atwood, L. Baldini, J. Ballet, G. Barbiellini, D. Bastieri, K. Bechtol, R. Bellazzini, et al., *Phys. Rev. Lett.* **116**, 151105 (2016).
 - [15] W. D. Apel et al., *Astropart. Phys.* **47**, 54 (2013), 1306.6283.
 - [16] S. Buitink et al., *Nature* **531**, 70 (2016), 1603.01594.
 - [17] M. G. Aartsen et al. (IceCube), *Phys. Rev. Lett.* **117**, 241101 (2016), 1607.05886.
 - [18] A. M. Hillas, *ARAA* **22**, 425 (1984).
 - [19] K. Murase, C. D. Dermer, H. Takami, and G. Migliori, *ApJ* **749**, 63 (2012), 1107.5576.
 - [20] A. Pe’er, K. Murase, and P. Meszaros, *Phys. Rev.* **D80**, 123018 (2009), 0911.1776.
 - [21] C. R. Kaiser and P. N. Best, *MNRAS* **381**, 1548 (2007), 0708.3733.
 - [22] J. Kataoka and L. Stawarz, *ApJ* **622**, 797 (2005), astro-ph/0411042.
 - [23] P. Bordas, V. Bosch-Ramon, and M. Perucho, *MNRAS* **412**, 1229 (2011), 1011.1653.
 - [24] J. A. Stevens, R. J. Ivison, J. S. Dunlop, I. R. Smail, W. J. Percival, D. H. Hughes, H. J. A. Röttgering, W. J. M. van Breugel, and M. Reuland, *Nature* **425**, 264 (2003), astro-ph/0309495.
 - [25] G. Brunetti and T. W. Jones, *International Journal of Modern Physics D* **23**, 1430007-98 (2014), 1401.7519.
 - [26] K. Murase and J. F. Beacom, *PRD* **81**, 123001 (2010), 1003.4959.
 - [27] M. De Domenico, M. Settimo, S. Riggi, and E. Bertin, *JCAP* **7**, 050 (2013), 1305.2331.
 - [28] F. Zandanel, I. Tamborra, S. Gabici, and S. Ando, *A&A* **578**, A32 (2015), 1410.8697.
 - [29] F. Shankar, D. H. Weinberg, and J. Miralda-Escudé, *MNRAS* **428**, 421 (2013), 1111.3574.
 - [30] P. Abreu et al. (Pierre Auger), *JCAP* **1305**, 009 (2013), 1305.1576.
 - [31] R. Alves Batista, A. Dundovic, M. Erdmann, K.-H. Kampert, D. Kuempel, G. Müller, G. Sigl, A. van Vliet, D. Walz, and T. Winchen, *JCAP* **5**, 038 (2016), 1603.07142.
 - [32] K. Kotera and M. Lemoine, *PRD* **77**, 023005 (2008), 0706.1891.
 - [33] K. Fang and A. V. Olinto, *ApJ* **828**, 37 (2016), 1607.00380.
 - [34] K. Werner, F.-M. Liu, and T. Pierog, *Phys. Rev. C* **74**, 044902 (2006).
 - [35] A. Mücke, R. Engel, J. P. Rachen, R. J. Protheroe, and T. Stanev, *Computer Physics Communications* **124**, 290 (2000), astro-ph/9903478.
 - [36] A. J. Koning and M. Duijvestijn, <http://www.talys.eu/http://www.talys.eu/> (2013).
 - [37] J. Tinker, A. V. Kravtsov, A. Klypin, K. Abazajian, M. Warren, G. Yepes, S. Gottlöber, and D. E. Holz, *ApJ* **688**, 709-728 (2008), 0803.2706.
 - [38] R. K. Sheth and G. Tormen, *MNRAS* **308**, 119 (1999), arXiv:astro-ph/9901122.
 - [39] A. Jenkins, C. S. Frenk, S. D. M. White, J. M. Colberg, S. Cole, A. E. Evrard, H. M. P. Couchman,

- and N. Yoshida, MNRAS **321**, 372 (2001), arXiv:astro-ph/0005260.
- [40] M. S. Warren, K. Abazajian, D. E. Holz, and L. Teodoro, Astrophys. J. **646**, 881 (2006), astro-ph/0506395.
 - [41] A. H. Gonzalez, S. Sivanandam, A. I. Zabludoff, and D. Zaritsky, Astrophys. J. **778**, 14 (2013), 1309.3565.
 - [42] H. Takami and K. Murase, Astrophys. J. **748**, 9 (2012), 1110.3245.
 - [43] V. S. Berezinsky, P. Blasi, and V. S. Ptuskin, Astrophys. J. **487**, 529 (1997), astro-ph/9609048.
 - [44] K. Murase and J. F. Beacom, JCAP **1302**, 028 (2013), 1209.0225.
 - [45] K. Murase, D. Guetta, and M. Ahlers, Phys. Rev. Lett. **116**, 071101 (2016), 1509.00805.
 - [46] K. Murase, J. F. Beacom, and H. Takami, JCAP **1208**, 030 (2012), 1205.5755.
 - [47] S. Inoue, F. A. Aharonian, and N. Sugiyama, Astrophys. J. **628**, L9 (2005), astro-ph/0505398.
 - [48] K. Murase (2015), 1511.01590.
 - [49] N. Senno, P. Mszros, K. Murase, P. Baerwald, and M. J. Rees, Astrophys. J. **806**, 24 (2015), 1501.04934.
 - [50] H. Kang, D. Ryu, and T. W. Jones, Astrophys. J. **456**, 422 (1996), astro-ph/9507113.
 - [51] S. Inoue, G. Sigl, F. Miniati, and E. Armengaud (2007), astro-ph/0701167.
 - [52] D. Kushnir, B. Katz, and E. Waxman, JCAP **0909**, 024 (2009), 0903.2275.
 - [53] U. Keshet (2010), 1011.0729.
 - [54] T. M. Kneiske, T. Bretz, K. Mannheim, and D. H. Hartmann, A&A **413**, 807 (2004), astro-ph/0309141.
 - [55] V. S. Berezinsky and G. T. Zatsepin, Phys. Lett. **B28**, 423 (1969).
 - [56] K. Greisen, Physical Review Letters **16**, 748 (1966).
 - [57] G. T. Zatsepin and V. A. Kuz'min, Soviet Journal of Experimental and Theoretical Physics Letters **4**, 78 (1966).
 - [58] M. Ahlers and F. Halzen, Phys. Rev. **D86**, 083010 (2012), 1208.4181.
 - [59] M. Ahlers and J. Salvado, Phys. Rev. **D84**, 085019 (2011), 1105.5113.
 - [60] G. Decerprit and D. Allard, Astron. Astrophys. **535**, A66 (2011), 1107.3722.
 - [61] V. S. Berezinsky and A. Yu. Smirnov, Astrophys. Space Sci. **32**, 461 (1975).
 - [62] X.-Y. Wang, R.-Y. Liu, and F. Aharonian, Astrophys. J. **736**, 112 (2011), 1103.3574.
 - [63] M. Lisanti, S. Mishra-Sharma, L. Necib, and B. R. Safdi, Astrophys. J. **832**, 117 (2016), 1606.04101.
 - [64] The Pierre Auger Collaboration, A. Aab, P. Abreu, M. Aglietta, I. A. Samarai, I. F. M. Albuquerque, I. Allekotte, A. Almela, J. Alvarez Castillo, J. Alvarez-Muñiz, et al., ArXiv e-prints (2016), 1612.07155.
 - [65] Pierre Auger Collaboration, JCAP **2**, 026 (2013), 1301.6637.
 - [66] S. Ostapchenko, Nucl.Phys.Proc.Suppl. **175-176**, 73 (2008), hep-ph/0612068.
 - [67] E.-J. Ahn, R. Engel, T. K. Gaisser, P. Lipari, and T. Stanev, Phys.Rev. **D80**, 094003 (2009), 0906.4113.
 - [68] A. M. Taylor, M. Ahlers, and F. A. Aharonian, Phys.Rev. **D84**, 105007 (2011), 1107.2055.
 - [69] K. Fang, K. Kotera, and A. V. Olinto, ApJ **750**, 118 (2012), 1201.5197.
 - [70] K. Murase, Y. Inoue, and C. D. Dermer, PRD **90**, 023007 (2014), 1403.4089.

Appendix A: Methods

Cosmic rays can be accelerated by black hole jets by mechanisms such as shock acceleration, shear acceleration, and magnetic reconnection. After escaping from the jet and lobe/bubble, cosmic rays rectilinearly or diffusively propagate in the turbulent magnetic field of the host cluster (or group). The semi-diffusive propagation is implemented based on the public UHECR propagation code CRPropa3 [31]. The diffusive propagation is computed semi-analytically by letting particles random walk with a step size equal to the coherence length of the magnetic field. The numerical step size is then converted to an actual trajectory length through the on-site diffusion coefficient [32, 33]. Interactions between nuclei and target nucleons of the ICM gas are computed using pre-tabulated cross sections and products that were calculated with the hadronic interaction model EPOS [34]. Photopion productions (photodisintegration) due to interactions between cosmic-ray protons (nuclei) and the infrared background of clusters are computed based on SOPHIA [35] (TALYS [36]) through CRPropa3.

We simulate host clusters in 10 mass bins from $M_{\min} = 5 \times 10^{13} M_{\odot}$ to $M_{\max} = 10^{16} M_{\odot}$, and 14 redshift bins from $z_{\min} = 0.005$ to $z_{\max} = 5$. The result, however, barely depends on M_{\max} and z_{\max} since the population of massive clusters at high redshifts is negligible. The minimum redshift $z_{\min} = 0.005$ corresponds to the distance of the Virgo cluster at ~ 20 Mpc. The halo mass function is calculated by

$$\frac{dn}{dM}(M, z) = f(\sigma) \frac{\rho_m}{M} \frac{d \ln \sigma^{-1}}{dM} \quad (\text{S1})$$

where $\rho_m(z) = \rho_m(0) (1+z)^3$ is the mean density of the universe at given redshift, and $\sigma(M, z)$ is the variance of the linear density field smoothed on a top-hat window function $r_t = (3M/4\pi\rho_m)^{1/3}$ [37]. For $f(\sigma)$, we adopt the Sheth-Tormen mass function multiplicity [38], which is consistent with results from N-body cosmological simulations [37, 39, 40].

The density profile of the intracluster medium gas in a cluster is normalized by $f_b M / (\mu m_p) = \int n_{\text{ICM}}(r) dV$, where $f_b = 0.13 M_{14}^{0.16}$ is the average baryon fraction of galaxy clusters [41], $\mu \approx 0.61$ is the mean molecular weight, and m_p is the mass of a proton. The infrared background photons in the cluster is modeled following reference [42], with a spectral energy distribution resulting from the superposition of the emission of 100 giant elliptical galaxies, and a density profile following the ICM gas distribution. The infrared background of the cluster add to the CMB and the EBL as target radiation fields. While not only radio-loud AGN but also radio-quiet AGN have been suggested as UHECR accelerators [20], the former objects are known to be more powerful. Radio-loud AGN are more common as a central galaxy in cool core clusters than in non-cool core clusters. To be conservative, we have not taken into account the high densities at the center of the subset of clusters that have cool cores [9].

Galaxy clusters and groups are gigantic reservoirs of cosmic rays and dark matter [43, 44]. Our simulations allow us to approximately calculate spectra of neutrinos and cosmic rays for a steady injection over a duration $t_{\text{inj}} \sim 1 - 10$ Gyr. The history of injections from AGNs is time-dependent and is dominated by their past activities at $z \sim 1 - 2$. Considering this effect, we have adopted $t_{\text{inj}} = 2$ Gyr. Two effects induce a spectral steepening in our model. First, a spectral break due to the escape of cosmic rays occurs at sufficiently high energies when $t_{\text{diff}}(E) < t_{\text{inj}}$ [8, 11]. In addition, a break in the injection spectrum is caused by the confinement of cosmic rays in the cocoon. Figure S1 demonstrates that $t_{\text{inj}} = t_H$, where $t_H = 13.75$ Gyr is the age of the Universe, leads to similar results. Thus for our fiducial parameters, our results are insensitive to changes in t_{inj} which affects the confinement ability of the cluster. In essence, since we achieve $s < s_{\text{acc}}$ (where s is the injection spectral index), our model is consistent with model-independent bounds on cosmic-ray reservoir scenarios, in which the injection spectral index, s , is constrained by the

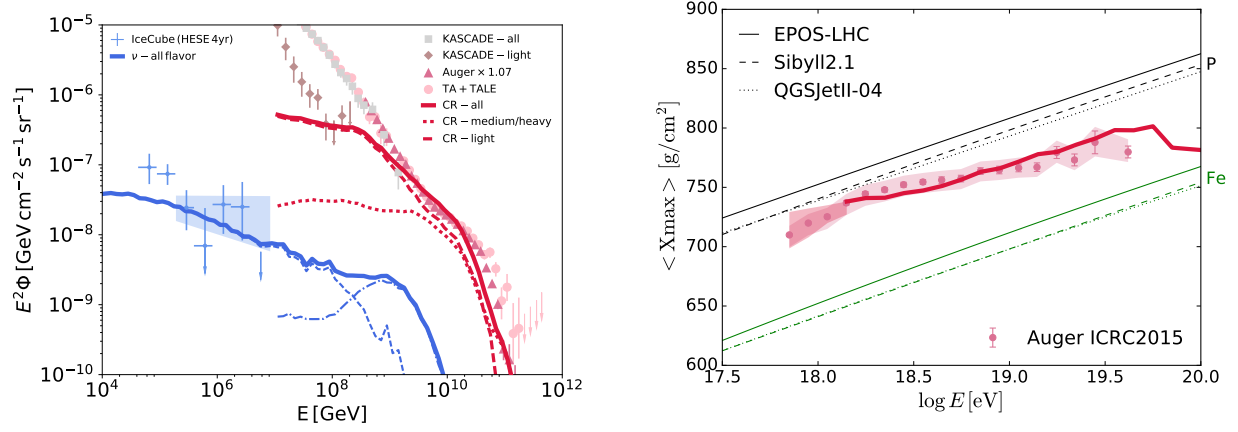


FIG. S1: Spectra of cosmic rays and neutrinos from reservoirs with black hole jets. Same as in the fiducial mixed-composition scenario but with the cosmic-ray injection time $t_{\text{inj}} = t_H$.

γ -ray background to be smaller than $s \sim 2.1 - 2.2$ [11].

All cosmic rays and neutrinos, including the primary cosmic ray particles injected into the simulation and their secondary and higher-order products, are tracked down to 1 TeV. The neutrino spectrum below this energy is extrapolated based on a spline fit to the simulation results between 2.2 TeV and 10 TeV. From the neutrino spectrum we obtain the spectrum of their γ -ray counterparts by [45]

$$E_\gamma Q_{E_\gamma} \approx \frac{2}{3} (E_\nu Q_{E_\nu})|_{E_\nu=E_\gamma/2}, \quad (\text{S2})$$

where EQ_E is the energy generation rate, and γ -ray and neutrino energies are related as $E_\gamma \approx 2E_\nu$. Then we take into account electromagnetic cascades during the intergalactic propagation by solving transport equations [46]. Note that clusters and groups are expected to be transparent up to ~ 100 TeV energies [44, 47].

As considered in this work, particle acceleration in a galaxy cluster and group is naturally expected in powerful intracluster sources such as black hole jets, which may include radio-loud AGNs and perhaps radio-quiet AGNs [48]. In principle, cosmic-ray accelerators may be powerful transients in galaxies including γ -ray bursts, supernova explosions, fast-rotating pulsars, and tidal disruption events [49]. In addition, particle acceleration can also happen in the accretion shocks that are commonly found at the outskirts of large-scale structures [50, 51]. Cosmic rays accelerated by accretion shocks can contribute to the second knee, and neutrinos have been suggested as a probe of such a scenario [8]. The accretion shock contribution is expected to be more important for massive clusters, and the corresponding neutrino production has been subject to various constraints [2, 33, 52]. In contrast, the contribution from internal accelerators such as AGNs is more important for less massive clusters, due to the fact that the population of such clusters is higher, and that AGNs are found to have a strong redshift evolution [9, 11]. The distribution of higher-energy cosmic rays is more uniform, which is favored by observations [53].

For the extragalactic propagation, we use CRPropa3 and take into account the photomeson and photodisintegration interactions between cosmic rays and background photons including the CMB and the EBL [54], as well as the decay of unstable intermediate products and the Bethe-Heitler production of electron-positron pairs. Cosmogenic neutrinos [55] are generated by photomeson interactions of protons above the Greisen-Zatsepin-Kuzmin energy [56, 57] ($E_{\text{GZK}} \sim 6 \times 10^{19}$ eV) during their intergalactic propagation. The flux of cosmogenic neutrinos is lower if UHECRs are

dominated by intermediate or heavy nuclei, as opposed to the pure proton composition [1, 26, 58]. Cosmogenic γ rays from intermediate and heavy nuclei are dominated by the Bethe-Heitler pair production [19, 59, 60]. It is known that cosmogenic γ rays has a universal spectral shape, and that its flux is basically determined by the energy injection rate of cosmic rays at ultrahigh energies [46, 61, 62]. For demonstration purposes, the total contribution to the EGB is estimated by adding the cosmogenic γ -ray flux of a mixed composition scenario [60] to the source γ rays obtained in this work. As in the simplest grand-unified model [2], the total γ -ray flux from our model is compatible to the non-blazar component of the EGB, which is about 10 – 30% of the total EGB [14, 63].

The default parameters are set to be $E_{\max}/Z = 10^{19.4}$ eV, $s_{\text{acc}} = 2.3$, and a proton fraction of $f_p = 83\%$. While the chosen values of the spectrum parameters are motivated by black hole jets of radio-loud and radio-quiete AGNs [19, 20], and f_p is determined by the fit to $\langle X_{\max} \rangle$, our results are not very sensitive to small variations of these parameters. Generally a softer cosmic-ray spectrum also leads to a softer neutrino spectrum, and with the same f_p , larger E_{\max} values lead to higher fluxes of cosmogenic neutrinos. For simplicity, only two elements (H and Fe) are included in the injection. Adding more intermediate elements can potentially provide a better fit to data. However, considering the large uncertainties in both observation and interpretation of the X_{\max} data, such a study is beyond the scope of this work, which aims at demonstrating the connection among multi-messengers with the basic parameters. Readers may refer to reference [64] for a dedicated fitting.

Appendix B: Proton Scenario

So far we have mainly focused on a mixed composition scenario, but the interpretation for the chemical composition of UHECRs is under debate. While three interaction models, EPOS [65], QGSJET [66] and SIBYLL [67] are commonly used, hadronic interaction models at the highest energies are based on the extrapolation from experimental data at lower energies, and thus still suffer from non-negligible uncertainties. A simultaneous fit to the Auger spectrum, $\langle X_{\max} \rangle$ and $\sigma(X_{\max})$ suggests the dominance of intermediate or heavier nuclei at the sources [64, 68], which is quite challenging for known astrophysical sources. Reference [64] also finds a main minimum and a second minimum in their fitting. The main minimum requires a very hard injection spectral index $s = 0.9$, which is different from typical expectations from the diffusive shock acceleration mechanism. The second minimum suggests $s = 2.0$ and is similar to the mixed composition scenario shown here, but with a $\sigma(X_{\max})$ lighter than the Auger measurements between $10^{18.8}$ eV and $10^{19.4}$ eV. The UHECR composition can also be modified by interactions inside cosmic-ray accelerators [19, 69, 70]. More quantitative discussion on the composition is beyond the scope of this work, and we do not attempt to fit to the $\sigma(X_{\max})$ data.

Below we consider an alternative scenario, where cosmic rays from radio-loud AGNs are dominated by pure protons (*aka* the “proton scenario”). Such a possibility is shown in Figure S2 for the completeness of our demonstration, since it has been argued that X_{\max} measurements by TA may be consistent with the light composition [4]. Like in the mixed-composition scenario, the neutrino products from the ICM is comparable to the 0.1-1 PeV measurements by IceCube. The difference between a nucleus and a proton in neutrino production can be very roughly estimated as follows. Considering that the inelastic cross section of a nucleus with mass number A scales as $\sigma_{Np} \sim A^{-1/3} \sigma_{pp}$, and that a nucleus with $Z \times E$ experiences the same level of diffusion as a proton with E , the interaction between the nucleus and the ICM gas has an effective optical depth $f_{Np} \sim A^{-1/3} f_{pp}$. Therefore, a neutrino product from a nucleus and that from a proton with Z times lower energy have an energy ratio $Z/A \sim 0.5$ and an energy flux ratio f_{Np}/f_{pp} .

Except for a different composition, we adopt the same injection spectrum, $dN/dE \propto E^{-2.3}$ and the same maximum energy, $E_{\max} = 10^{20.8}$ eV, as in our mixed composition case. One feature of the

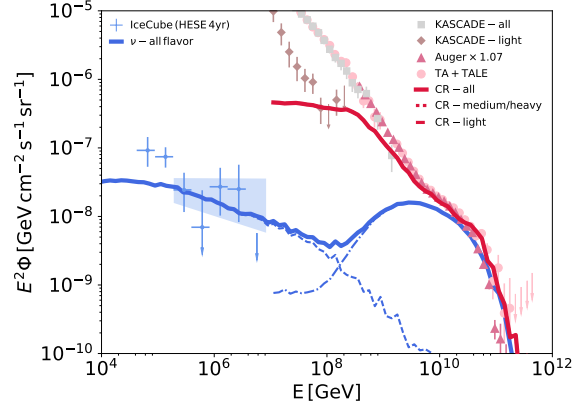


FIG. S2: Spectra of cosmic rays and neutrinos from reservoirs with black hole jets, assuming that all cosmic rays are protons with $E_{\text{max}} = 10^{20.8}$ eV. The propagated cosmic ray spectrum (solid red) matches the Auger and TA data above the ankle ($\sim 10^{18.5}$ eV).

proton scenario is the presence of a prominent EeV neutrino bump due to a copious production of cosmogenic neutrinos. The energy flux level of neutrinos is still consistent with the current upper limits posed by the non-detection of extremely high-energy neutrinos in the IceCube data [17], but should be detectable in the near future. In the classical ankle scenario with $s = 2.0$, the diffuse isotropic γ -ray flux is shown to be comparable to the non-blazar component of the EGB [2]. Our proton scenario with $s_{\text{acc}} = 2.3$ effectively leads to $s \sim 2$, but the tension with the γ -ray data is slightly stronger due to more cosmogenic γ -ray production.